LBL-26896
Preprint

Lawrence Berkeley Laboratory

UNIVERSITY OF CALIFORNIA

Materials & Chemical Sciences Division

Submitted to Journal of the Electrochemical Society

Mathematical Modeling of the Sodium/Iron Chloride Battery

M. Sudoh and J. Newman

March 1989

Prepared for the U.S. Department of Energy under Contract Number DE-AC03-76SF00098.

DISCLAIMER

LBL-26896

Mathematical Modeling of the Sodium/Iron Chloride Battery

Masao Sudoh and John Newman

Department of Chemical Engineering
University of California

and

Materials and Chemical Sciences Division
Lawrence Berkeley Laboratory
1 Cyclotron Road
Berkeley, CA 94720

LBL-26896

Mathematical Modeling of The Sodium/Iron Chloride Battery

Masao Sudoh[†] and John Newman

Materials and Chemical Sciences Division, Lawrence Berkeley Laboratory, and Department of Chemical Engineering, University of California, Berkeley, California 94720

March 10, 1989

Abstract

A mathematical model of the sodium/iron chloride battery containing a molten $AlCl_3$-NaCl electrolyte is presented. A cylindrical cell consisting of a positive iron electrode, an electrolyte reservoir, a separator, and a negative sodium electrode is considered. The analysis uses concentrated-solution theory within the framework of a macroscopic porous electrode model. The effects of the state of discharge, the cell temperature, the precipitation and dissolution rates of NaCl, and the current density on the current-potential relation during the discharge and charge cycles are discussed. The major influences on battery performance are changes in porosity and component volume fractions during cycling.

Introduction

Na/β''-$Al_2O_3/NaAlCl_4$/Metal chloride batteries are being developed for load-leveling and electric vehicle applications [1-5]. This battery

---

[†]Present Address: Department of Chemical Engineering, Shizuoka University, Hamamatsu, Japan 432

Key words: porous electrode, molten salt electrolyte, cell performance, mathematical modeling, precipitation

is similar to the sodium/sulfur cell, with the sulfur electrode being replaced by a metal/metal chloride electrode. This battery operates between 170 and 350°C with a molten sodium tetrachloroaluminate ($NaAlCl_4$) electrolyte. These lower temperatures reduce corrosion, which is a problem in Na/S batteries. The melt composition varies with the apparent concentration ratio of NaCl to $AlCl_3$. To prevent electrode material and products from dissolving into the electrolyte, a NaCl-rich melt has been adopted. In NaCl-rich melts, the precipitation of NaCl and its effect on electrode kinetics must be accounted for.

Developments in the theory of flooded porous electrodes were reviewed by Newman and Tiedemann [6]. Porous electrodes containing sparingly soluble reactants have been investigated for systems such as the Ag-AgCl and Cd-$Cd(OH)_2$ couples [7], the zinc electrode [8], and the lead dioxide electrode [9, 10]. A model describing the cell behavior for a complete cell has been developed. The lead-acid cell [11, 12], the LiAl/FeS molten salt battery [13], and the Li/$SOCl_2$ primary cell [14, 15] have been analyzed in detail.

Mathematical modeling is used to predict phenomena which are difficult to observe experimentally and to identify factors important to battery performance. In battery modeling, a major goal is to predict the cell potential for a given constant current as a function of the state of discharge. When the concentration of the electrolyte varies during the discharge and charge cycle, the potential profile in the electrolyte phase must be described by a modified Ohm's law. The precipitates that are produced during the electrode reaction affect the rate of the reaction by covering the active sites and affect the performance by plugging

the porous electrode.

In this paper, a mathematical model of a $Na/FeCl_2$ battery with a molten $AlCl_3$-NaCl electrolyte is presented. The cell performance of a complete cell is analyzed using a macroscopic theory of porous electrodes. The transport equations are based on concentrated-solution theory. Factors affecting the cell behavior are discussed.

Model Development

A schematic diagram of the $Na/FeCl_2$ battery is shown in Fig. 1. A one-dimensional, cylindrical model describes this system. The cell consists of a positive ($Fe/FeCl_2$) electrode, an electrolyte reservoir, a separator (β"-alumina), and a negative (Na^+/Na) electrode. The positive electrode is fabricated from sintered iron which is partly chlorinated chemically or electrochemically. The conversion of iron to iron chloride is less than 30 percent so that the matrix remains electrically conductive [3].

The electrolyte is a molten $AlCl_3$-NaCl salt saturated with NaCl and can be treated as a concentrated mixture of Na^+, $AlCl_4^-$ and Cl^- [16]. The transport equation for two binary molten salts with a common ion was presented by Pollard and Newman [17]. To use their analysis, the salts A and B are respectively $NaAlCl_4$ and NaCl, and the species 1, 2 and 3 are $AlCl_4^-$, Cl^-, and Na^+.

A single electrode reaction can be represented by

$$\sum_i s_i M_i^{z_i} \rightarrow ne^- . \qquad (1)$$

The electrode reaction on the positive electrode is

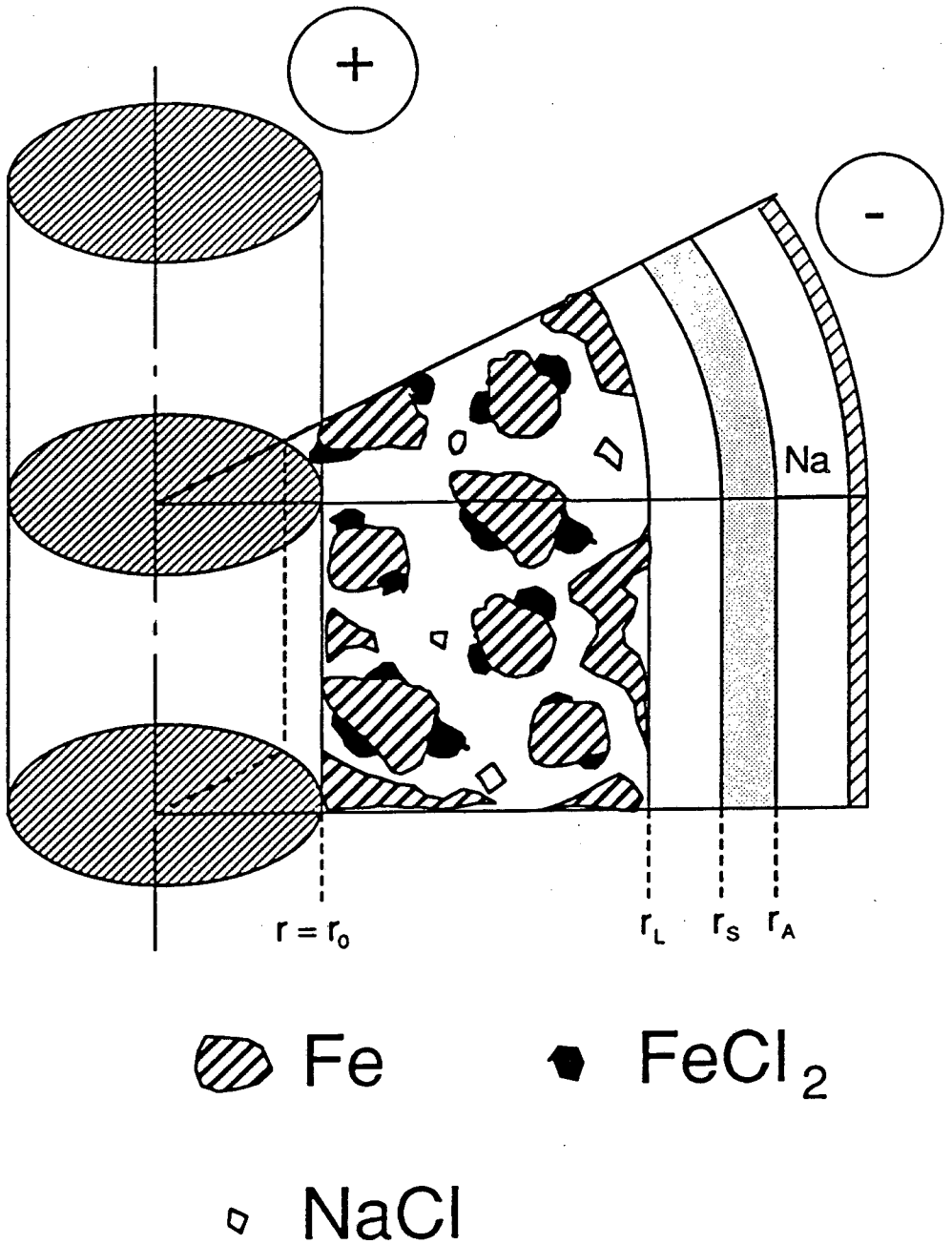

Figure 1. Schematic diagram of sodium/iron chloride battery.

$$Fe + 2\ Cl^- - FeCl_2 \longrightarrow 2\ e^-. \tag{2}$$

However, the actual reactant of the discharge might be the ferrous complex ions, FeX_m^{-m+2}. If X^- is $AlCl_4^-$, the complex is $Fe(AlCl_4)_4^{-2}$.

In the melt saturated with NaCl, a chemical reaction accompanies the electrode reaction:

$$Na^+ + Cl^- \rightleftarrows NaCl. \tag{3}$$

The general equations of ionic transport and a modified Ohm's law are given by Pollard and Newman [17]. In the absence of double-layer charging, the transfer rate, aj_{in}, of species i from the metal phase to the electrolyte phase is

$$aj_{in} = -\frac{s_i}{nF}\nabla\cdot i_2 + s_{i,I}\,R_I, \tag{4}$$

where R_I is the reaction rate for the precipitation and dissolution of NaCl and is described by

$$R_I = k_p\left[\frac{1 - x_A}{\bar{V}_e^2} - K_{sp}\right], \tag{5}$$

where K_{sp} is the solubility product. The porosity of the positive electrode varies according to

$$\frac{\partial\epsilon}{\partial t} = \sum_i\left[\frac{s_i'\,\bar{V}_i}{nF}\nabla\cdot i_2 - s_{i,I}'\,\bar{V}_i\,R_I\right], \tag{6}$$

where s_i' and $s_{i,I}'$ are the stoichiometric coefficients for the solid phase.

The apparent current density I is based on the surface area of the separator using the inner diameter. When the total overpotential

$\eta = \phi_1 - \phi_2$ is introduced, the current density in the electrolyte phase is given by

$$i_2 = \frac{\sigma_e \kappa_e}{\sigma_e + \kappa_e} \left\{ \nabla\eta + \frac{r_S I}{\sigma_e r} + \frac{RTt_1^c}{F(1 - x_A)x_A} \left[1 + \frac{d \ln \gamma_A}{d \ln x_A} \right] \nabla x_A \right\}, \quad (7)$$

where $\kappa_e = \kappa\epsilon^{1+\tau}$ and $\sigma_e = \sigma\epsilon^{1+\tau}$ are estimated using the tortuosity factor τ.

Since $c_3 = c_T/2$, the transference number of sodium ion, t_3^* is assumed to be 0.5. A material balance for species i gives the change in the mole fraction x_A with time:

$$\epsilon \frac{\partial x_A}{\partial t} = \bar{V}_e x_A R_I + \bar{V}_e x_A \frac{\nabla \cdot i_2}{F} v^* \nabla x_A + D\nabla \cdot (\epsilon^{1+\tau} \nabla x_A) \quad (8)$$

$$- \frac{(\bar{V}_A - \bar{V}_B)}{\bar{V}_e} D\epsilon^{1+\tau} (\nabla x_A)^2,$$

where $\bar{V}_e$ is the average molar volume of the electrolyte:

$$\bar{V}_e = \sum_k x_k \bar{V}_k. \quad (9)$$

Using the material balance, the porosity change given by Eq. (6), and the relation that $c_A \bar{V}_A + c_B \bar{V}_B = 1$, the distribution of the molar average velocity in the porous electrode is governed by

$$\nabla \cdot v^* = - \nabla \cdot i_2 \left(\frac{\bar{V}_{Fe} - \bar{V}_{FeCl_2} + 2\bar{V}_B}{2F} \right) + (\bar{V}_p - \bar{V}_B) R_I \quad (10)$$

$$+ (\bar{V}_A - \bar{V}_B) \nabla \cdot \left[\epsilon^{1+\tau} D(c_A + c_B) \nabla x_A \right] + \frac{\bar{V}_A}{F} \nabla \cdot (t_1^* i_2) + \frac{\bar{V}_B}{F} \nabla \cdot (t_2^* i_2).$$

From the charge balance using the local transfer current j,

$$\nabla \cdot i_2 = j \tag{11}$$

Combination of Eqs. (A.1), (A.2) and (A.3) in the Appendix gives

$$j = \frac{\exp\left(\frac{\alpha_a F}{RT}\eta\right) - \exp\left(-\frac{\alpha_c F}{RT}\eta\right)}{\frac{1}{i_0 a_m} + \frac{1}{nFc_{r,e}}\left(\frac{1}{k_m a_m} + \frac{1}{k_s a_s}\right)\exp\left(-\frac{\alpha_c F}{RT}\eta\right)}. \tag{12}$$

During charge, the mass transfer rate of the complex ion from the bulk to the surface of the salt is assumed fast.

Equations (7), (8), and (10) to (12) are solved for the five unknowns, η, x_A, v^*, i_2, and j, using the numerical technique of Newman [18]. The initial and boundary conditions are described below.

The initial conditions before the first discharge are

$$x_A = x_{A,sat}, \tag{13}$$

$$v^* = \frac{\bar{V}_e - 2\bar{V}_B - \bar{V}_{Fe} + \bar{V}_{FeCl_2}}{2F} i_2. \tag{14}$$

The boundary conditions at the current collector of the positive electrode ($r = r_0$) are

$$\frac{d\eta}{dr} = -\frac{r_s I}{\sigma_e r_0}, \tag{15}$$

$$i_2 = 0, \tag{16}$$

$$\frac{dx_A}{dr} = 0, \tag{17}$$

$$v^* = 0. \tag{18}$$

The boundary condition at the interface between the positive electrode and the reservoir ($r = r_L$) is

$$i_2 = r_S I / r_L. \tag{19}$$

From the material balance of the ionic species in the reservoir,

$$\frac{\partial (V_R\, c_{Ri})}{\partial t} = A_L (N_i)_{r=r_L} - A_S (N_i)_{r=r_S} \tag{20}$$

where $A_L = 2\pi r_L H$ and $A_S = 2\pi r_S H$. The change in the electrolyte volume of the reservoir, V_R, with time is

$$\frac{\partial V_R}{\partial t} = - \frac{V_R}{c_{TR}} \frac{\partial c_{TR}}{\partial t} + A_L (v^*)_{r=r_L} - \frac{A_S I}{F c_{TR}} \tag{21}$$

where c_{TR} is the total concentration in the reservoir. By using the relation that $c_{TR} = (c_T)_{r=r_L} = 2/(\bar{V}_e)_{r=r_L}$, the above equation can be rewritten as a function of $(x_A)_{r=r_L}$. The change of x_A at $r = r_L$ with time is by,

$$V_R \frac{\partial x_A}{\partial t} = - A_L D \epsilon^{1+\tau} \nabla x_A. \tag{22}$$

For the negative electrode, the electrode reaction is thought to occur near the interface between the separator and the melt phase. Linear kinetics is assumed for this reaction [19]:

$$i = \frac{i_{0,N} F}{RT} \eta_N. \tag{23}$$

In the matrix phase, the potential gradient is

$$i_1 = - \sigma_e \nabla \phi_1 \tag{24}$$

where i_1 and ϕ_1 are the current density and the potential in the solid matrix.

When the reference electrode has a reaction of the same kind as the working electrode, the open circuit potential in the electrolyte unsaturated or supersaturated with NaCl differs by ΔU_P from the potential measured in the saturated solution,

$$\Delta U_P = \frac{RT}{F} \ln \frac{a_{2,sat}}{a_2}. \tag{25}$$

The terminal voltage U is

$$U = U_o + IR_{res} + IR_{sep} + \eta_N + (\phi_{1,P})_{r=r_0} - (\phi_{2,P})_{r=r_L} + (\Delta U_P)_{r=r_L} \tag{26}$$

where U_o is the open circuit voltage of the cell, R_{res} is the resistance of the electrolyte in the reservoir, and R_{sep} is the resistance of the separator.

Since this battery operates at relatively high temperatures, the rate of NaCl precipitation might be anticipated to be fast. For infinitely fast kinetics, the electrolyte solution is saturated, and no concentration gradient exists. Two simpler models were developed for this case. The first case (Model 2) assumes that the mass transfer is also fast, so that reactants are always present everywhere in the battery. The second model (Model 3) assumes that the mass transfer rates are slow, so that once the reactants are depleted in one part of the electrode, the reaction rate falls to zero. In this case, a very sharp reaction zone moves through the battery during discharge with greater and greater portions of the electrode becoming inactive.

If the NaCl precipitation kinetics is indeed very fast, these models can be viewed as extreme cases of the model discussed in detail above (Model 1), and discharge characteristics of Model 1 are expected

to be intermediate between those of these simpler models. Comparisons are made in the next section.

Results and Discussion

The parameters shown in Table 1 are used for the calculations. The dimensions of the battery were chosen to be consistent with the previous papers [1-5]: r_0 = 0.25 cm, r_L = 2.5 cm, r_S = 2.8 cm, r_A = 3.0 cm, and H = 30.0 cm. The sintered iron (porosity = 77 %) is chlorinated to the conversion f, which is 0.2 for most calculations. The initial volume fractions before discharge are: $\epsilon_{m0} = 0.23(1-f)$, $\epsilon_{s0} = 0.23f\bar{V}_{FeCl_2}/\bar{V}_{Fe}$, and $\epsilon_{p0} = 0.01$. The cell temperature is assumed to be constant. Data given by Boxall *et al.* [16] were used to determine equilibrium

Table 1. Parameters used in the calculations.

$\bar{V}_p$	[cm^3/mol]	27.0
$\bar{V}_{Fe}$	[cm^3/mol]	7.1
$\bar{V}_{FeCl_2}$	[cm^3/mol]	40.1
U_o	[V]	$2.524 - 3.51 \times 10^{-4} T$
$i_{0,ref}$	[A/cm^2]	1.0×10^{-4}
$i_{0,N}$	[A/cm^2]	5.0
$c_{r,ref} = c_{r,e}$		$c_{2,ref} = c_{2,sat}$
$\alpha_a = \alpha_c = 1$		$\beta = 0.5$
$\kappa_{sep} = 0.2\kappa$		$\tau = 0.5$

concentrations of $AlCl_4^-$, Cl^-, $Al_2Cl_7^-$, and $AlCl_3$. The solubility of NaCl in $NaAlCl_4$ melt was derived from the published data [20]. It is likely that the predominant Fe^{2+} species in this melt is chloroaluminate complexes. The solubility of $FeCl_2$ might be proportional to the concentration of $Al_2Cl_7^-$, according to the proposed reaction [21]

$$FeCl_2 + 2Al_2Cl_7^- \longrightarrow Fe(AlCl_4)_4^{2-}. \tag{27}$$

The ferrous complex concentration $c_{r,e}$ at equilibrium is assumed to be half of the concentration of $Al_2Cl_7^-$ and is estimated as 4.1×10^{-8} mol/cm^3 at 300°C. The activity ratio is replaced by the mole fraction ratio [22]. Transference numbers, t_1^c and t_2^c, are assumed to be x_A and x_B, respectively. Most calculations are carried out using the conditions: 30 mA/cm^2-discharge, 10 mA/cm^2-charge, and the temperature 300°C. The units of the k_p's shown in the figures are cm^3/mol·s.

Effect of k_p on electrolyte composition.—Figure 2 shows the distribution of the mole fraction of salt A, $NaAlCl_4$, in the positive electrode. The SOD in the figure refers to the state of discharge and is given by

$$SOD = \frac{-\int_0^t I\,dt}{c_{d,max}}, \tag{28}$$

where integration over time is performed beginning at a state of full charge. The radial distance from the current collector is normalized by the radial thickness of the porous electrode: $(r - r_0)/(r_L - r_0)$.

As shown in Eqs. (2) and (3), chloride ions are extracted from the electrolyte during charge, and this tends to raise the mole fraction of salt A. During discharge, the distribution of the mole fraction changes

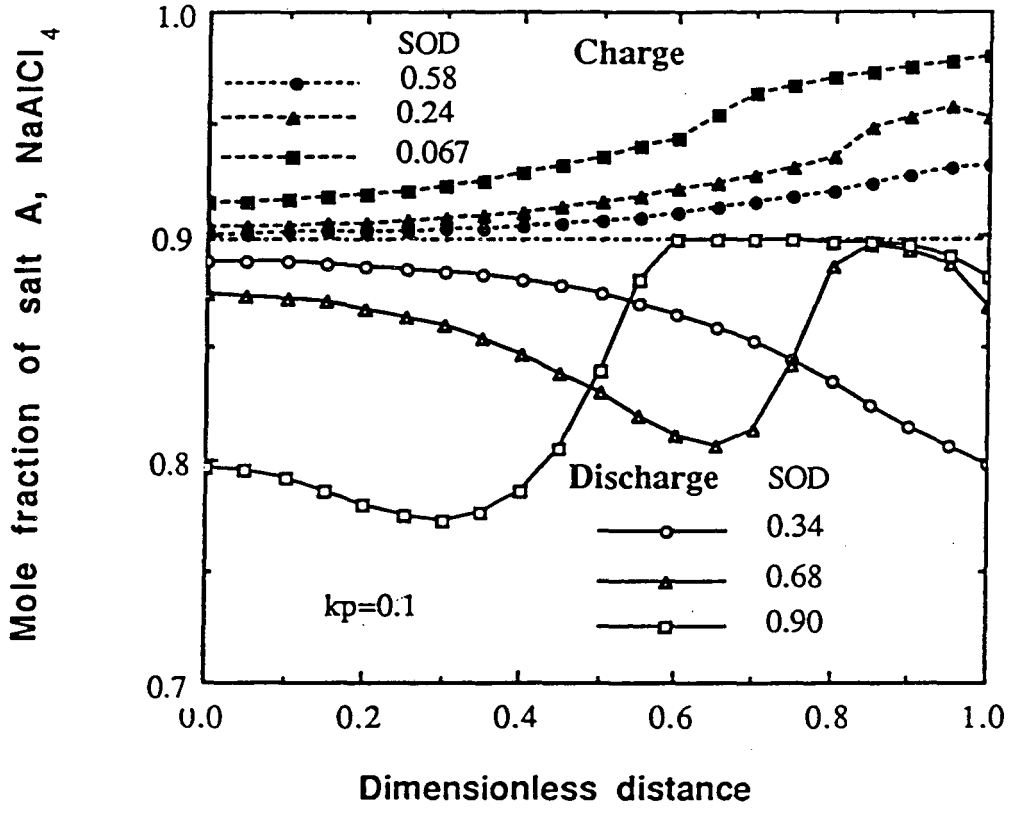

Figure 2. Mole fraction distribution of salt A, $NaAlCl_4$, in porous electrode for various states of discharge during discharge and charge.

with time, and the minimum value of x_A shifts inward from the electrode-reservoir interface. During charge, the mole fraction of salt A rises above the saturation value. That is, the chloride ion concentration decreases with time of charge.

Figure 3 shows the distribution of mole fraction of the electrolyte for different rate constants of precipitation and dissolution of NaCl. As k_p is increased, the mole fraction approaches the value at saturation. For the charging process, as k_p is increased, the mole fraction in the outer part of the electrode does not approach the value at saturation because the NaCl precipitate has disappeared in this region. The electrolyte composition in the inner part approaches saturation as the rate constant of NaCl dissolution increases.

Comparison with the model without concentration gradients.—Figure 4 shows the change in terminal voltage with the state of discharge for different values of k_p. The discharge capacity increases with decreasing k_p. The change in terminal voltage calculated with the assumption of no concentration gradient (Model 2) is also shown in this figure. (Models 2 and 3 are identical during discharge.) The analysis that includes the concentration gradients is Model 1. The change in voltage with the SOD approaches the results of Model 2 when k_p is larger than 0.1 $cm^3/mol \cdot s$. For the discharging process, the voltage increases initially and then gradually decreases. The voltage increment is larger for smaller k_p. When k_p is 0.01 $cm^3/mol \cdot s$, the charging voltage increases sharply.

To elucidate the effect of k_p on battery performance, the change in porosity with time is analyzed. Figure 5 shows the change in the

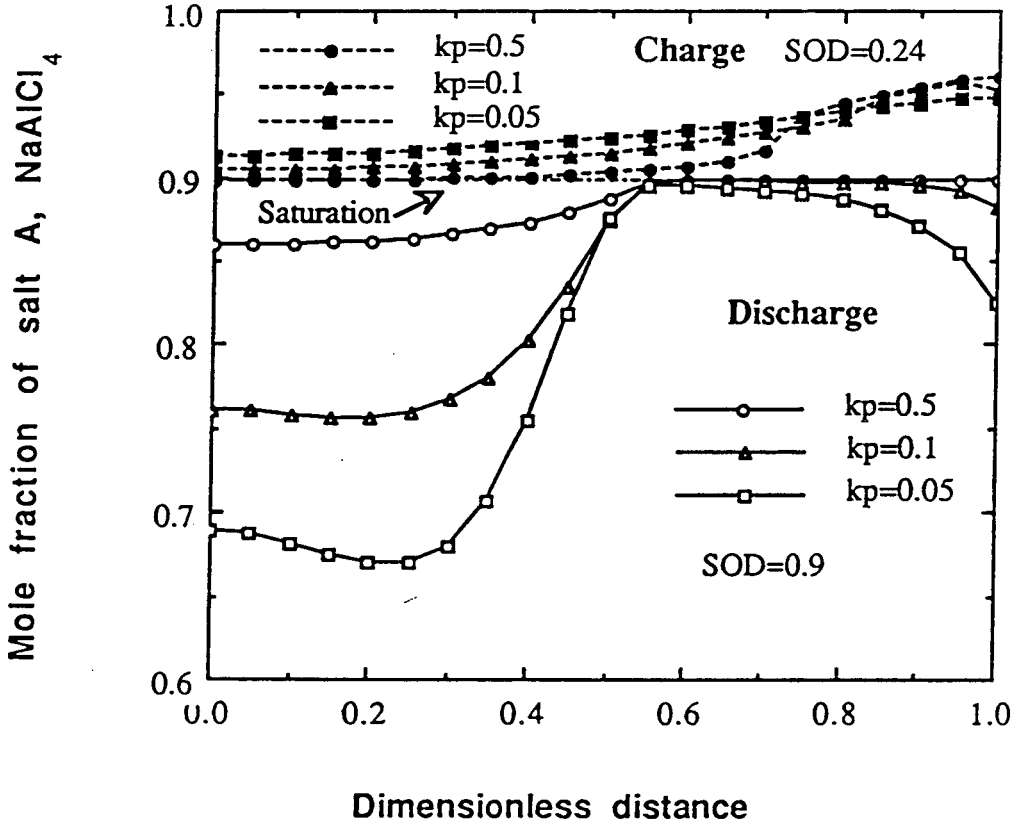

Figure 3. Mole fraction distribution of salt A in porous electrode for various rate constants of precipitation and dissolution of NaCl.

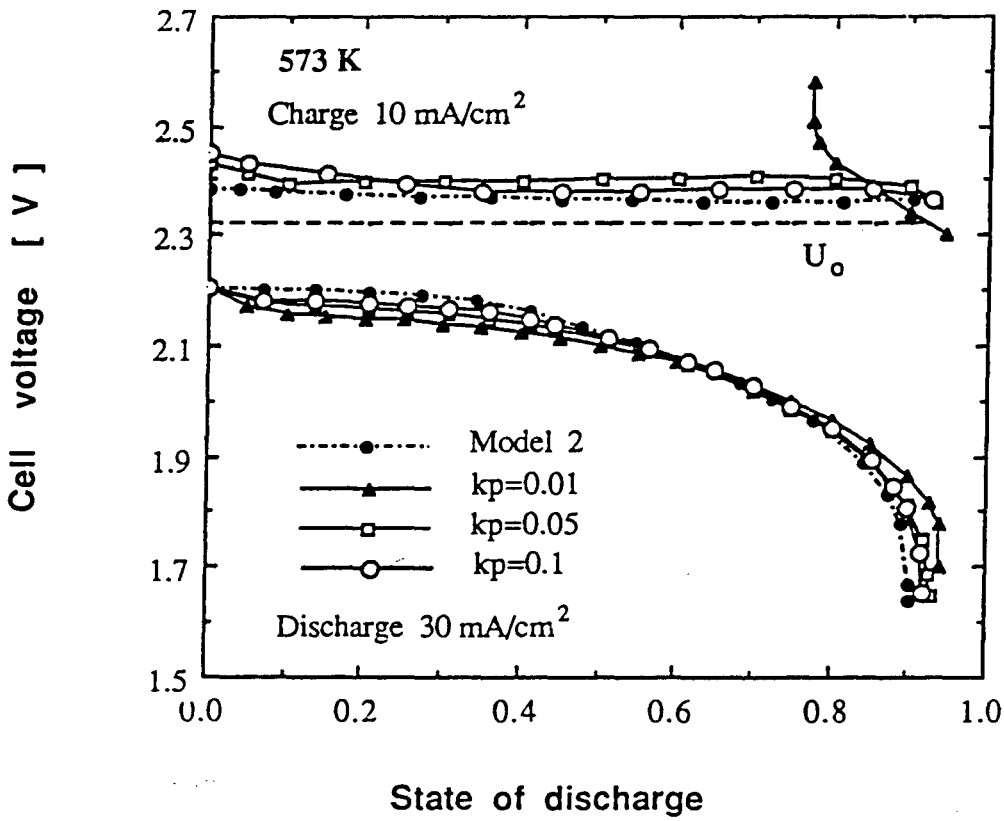

Figure 4. Voltage change with state of discharge during discharge and charge for different rate constants of precipitation and dissolution of NaCl.

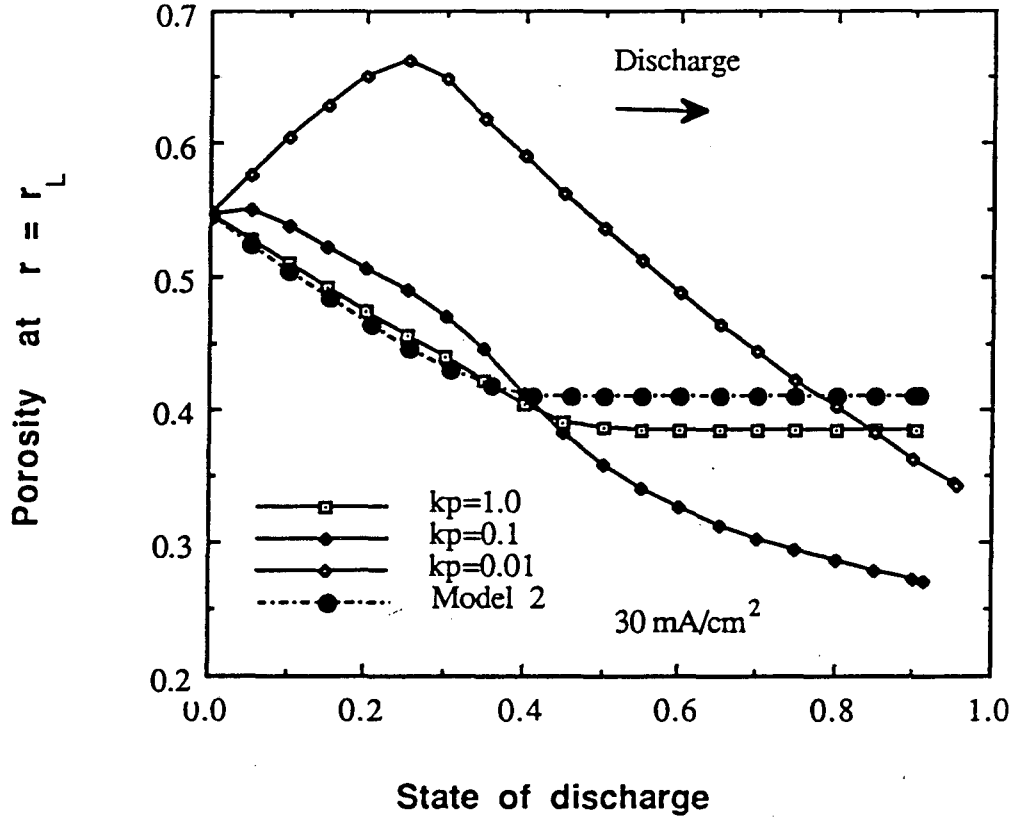

Figure 5. Change in porosity at $r = r_L$ with state of discharge during discharge for different rate constants of precipitation of NaCl.

porosity at the electrode-reservoir interface for different values of k_p. The change in porosity is caused by differences in the molar volumes of the solid species. Since the volume fraction of NaCl is affected by the rates of precipitation and dissolution, the porosity is also affected by these rates. The porosity at the interface decreases with the SOD, and the change in porosity with the SOD at large k_p is consistent with results calculated by Model 2. For small values of k_p, more or less supersaturation with NaCl occurs, and the porosity increases during the initial portion of the discharge.

Figure 6 shows the change in porosity during charge. When k_p is smaller than 0.1 $cm^3/mol \cdot s$, the porosity tends to decrease initially with decreasing SOD. Since the volume fraction of the NaCl precipitate changes little at the smaller k_p, the conversion of Fe to $FeCl_2$ decreases the porosity. When the SOD approaches about 0.8, the porosity gradually increases, because the dissolution rate gradually increases and the volume fraction of the NaCl precipitate decreases. When k_p is 0.01 $cm^3/mol \cdot s$, the pore at the electrode-reservoir interface plugs at earlier states of charge. When k_p is 1.0 $cm^3/mol \cdot s$, the changes in porosity are different, and the porosity has a larger value than that given by Model 2 for the fully charged state. The shift in electrolyte composition slows down the charging reaction near the pore mouth relative to that predicted by model 2 with no composition variation.

There is no information about the value of k_p. According to previous reports, the batteries do not plug at the charging current density of 10 mA/cm^2, which suggests that k_p is larger than 0.05 $cm^3/mol \cdot s$. To account for the disappearance of the NaCl precipitate, the calculation

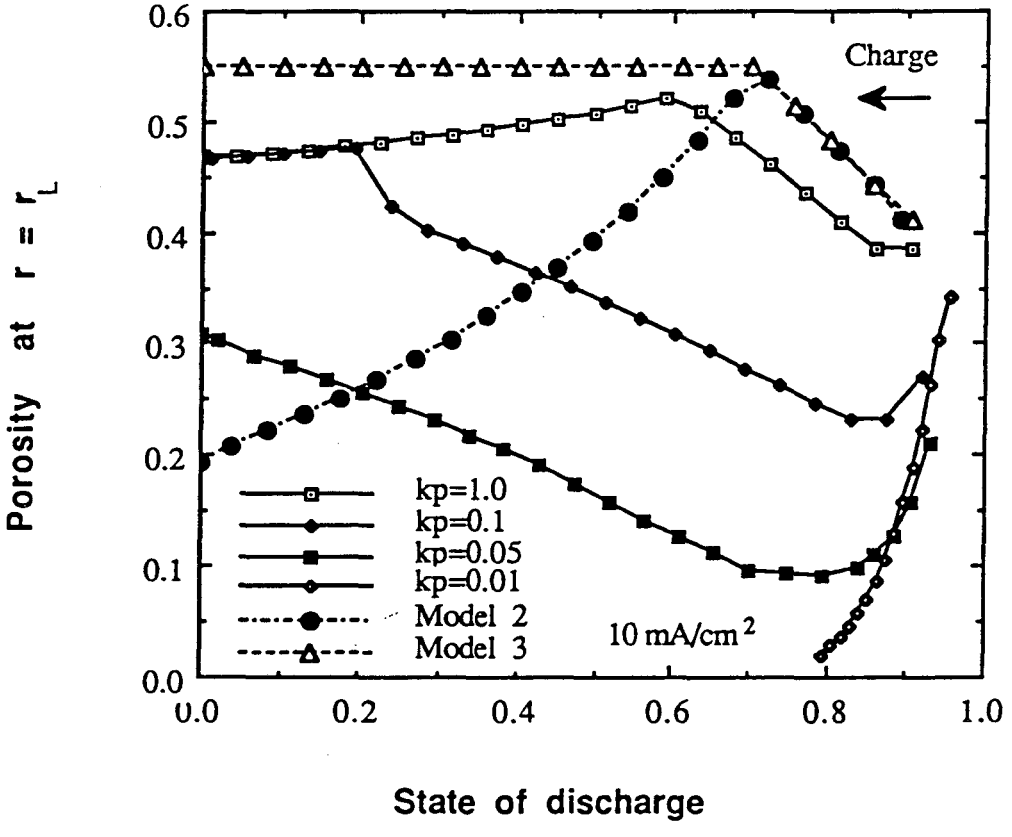

Figure 6. Change in porosity at r = r_L with state of discharge during charge for different rate constants of precipitation of NaCl.

is carried out with the assumptions that there are no concentration gradients and that the electrode reaction rate is cut off by the disappearance of the precipitate (Model 3). The porosity change predicted by Model 3 is shown in Fig. 6 and is close to the one calculated for k_p = 1.0 $cm^3/mol \cdot s$.

Transfer Current.—Figure 7 shows how the local transfer current j varies during discharge. The reaction distribution shifts toward the inner part of the electrode as the $FeCl_2$ reactant disappears. At the end of the discharge, the transfer current has its maximum near the positive current collector and more than half of the electrode is inactive. Therefore, the voltage drop at the end of the discharge is largely caused by the decrease in the active surface area of the positive electrode. The transfer current calculated by Model 1 using k_p = 1.0 $cm^3/mol \cdot s$ is close to that given by Model 2.

Figure 8 shows the comparison of the transfer currents calculated by the three models during charge. When the cell is close to full charge, the curves of the three models show quite different behavior. The transfer current given by Model 2 has its maximum at the outer part of the electrode, but the reaction distributions of Models 1 and 3 shift toward the inner part of the electrode. The chloride ion concentration has the distribution given in Figs. 2 and 3. In Model 1, the reaction rate decreases with decreasing Cl^- concentration because the exchange current density decreases and the open circuit potential increases. The value given by Model 1 is between those given by Model 2 and Model 3.

Effect of current density during charge.—According to previous papers [1-5], the charging current density should be relatively small.

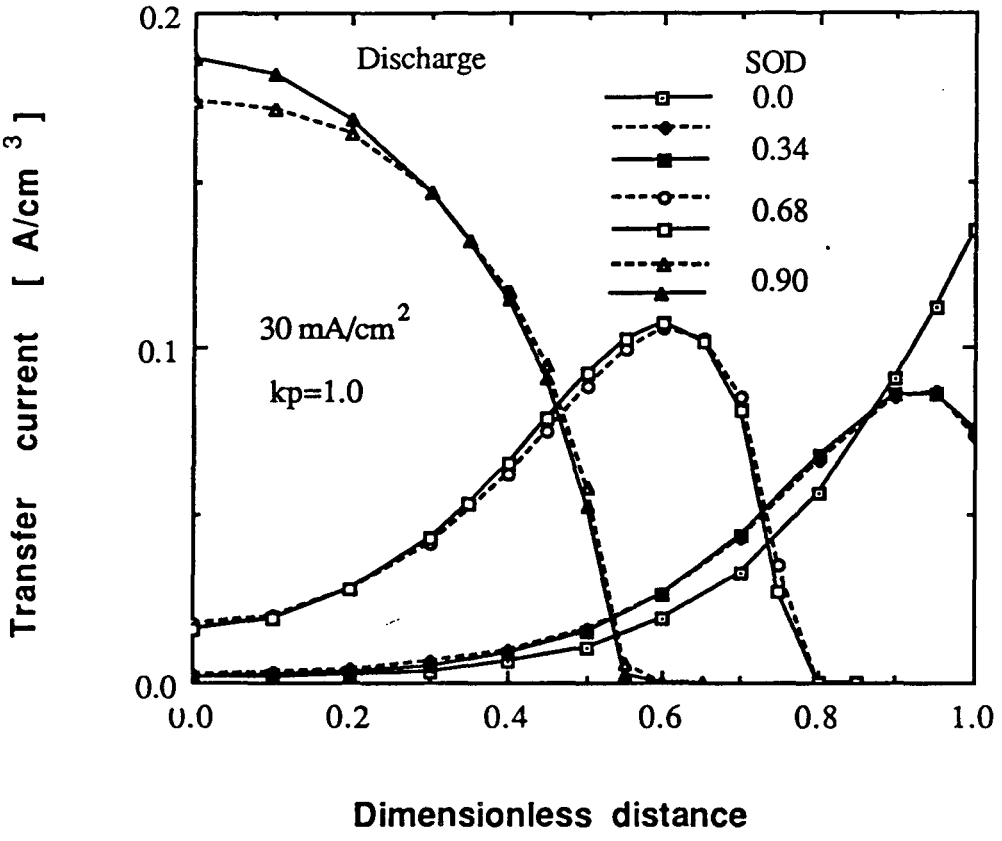

Figure 7. Local transfer current in the porous electrode during discharge. The broken and solid lines are results calculated by Model 1 and Model 2, respectively.

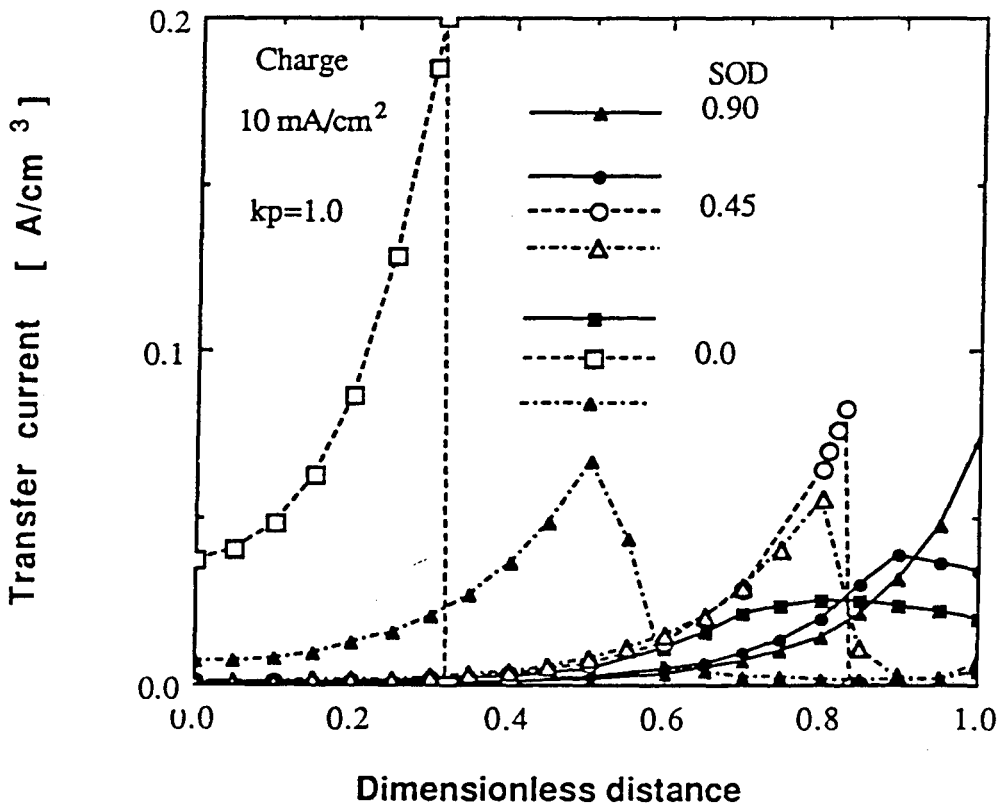

Figure 8. Comparison of local transfer currents calculated by different models during charge. The one-dotted, solid and broken lines are results calculated by Model 1, Model 2 and Model 3, respectively.

Figure 9 shows the change in cell voltage with the SOD as predicted by the different Models. The discharging current density is fixed at 30 mA/cm^2. When the charging current density is increased, the difference between the calculated values of the different models becomes greater. The potential at 50 mA/cm^2 predicted by Model 2 increases sharply at the latter stage of charge because of the plugging of the open pore in the porous electrode. The charging voltage gradually increases with decreasing SOD because of the decrease in the porosity and active surface area. The cell voltage calculated by Model 3 is close to the cell voltage calculated by Model 1. It might be preferable to adopt Model 3 as an alternative to Model 1, which requires more calculation.

Effect of temperature.—The electrolyte conductivity, the separator conductivity, the open circuit potential, the concentration of ferrous ion complex, and the saturation concentrations of the ionic species in the melt are functions of temperature. Figure 10 shows the effect of the operating temperature on the cell voltage. Normal operating temperatures are between 523 K and 573 K. It should be noted that the discharge capacity decreases with decreasing temperature.

Effect of chlorination conversion.—The porous electrode is made from iron that has been sintered and partially chlorinated. The initial porosity of the positive electrode is affected by the conversion of Fe to $FeCl_2$. Increasing the discharge capacity requires a high degree of chlorination and as full a discharge as possible. Figure 11 shows that the discharge capacity has its maximum near 0.3 chlorination conversion, where the porosity of the sintered iron is 0.77. This result agrees with a previous qualitative analysis [3].

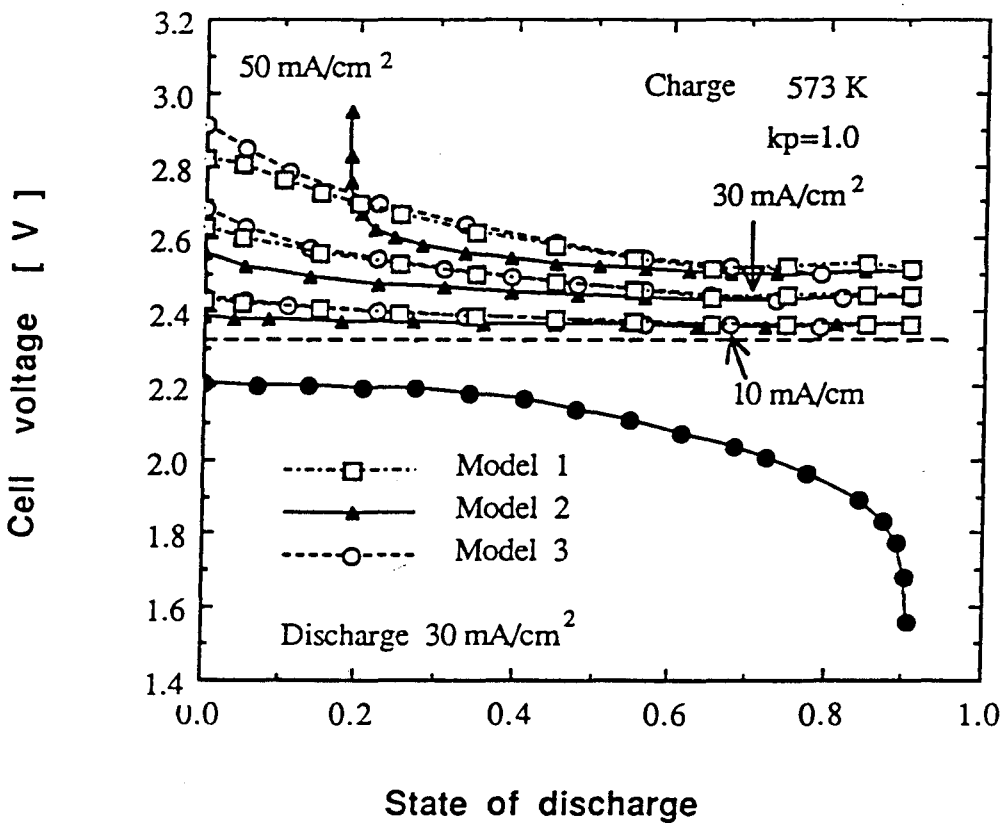

Figure 9. Comparison of terminal voltage changes with state of discharge, calculated by different models.

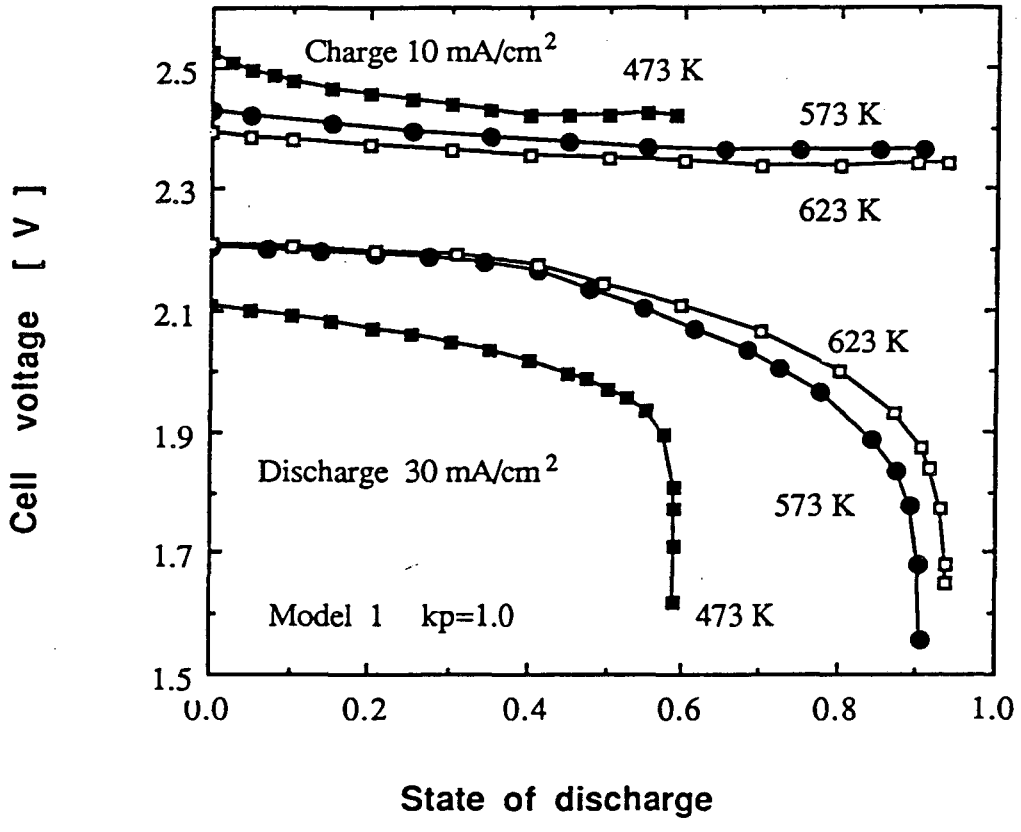

Figure 10. Effect of operating temperature on terminal voltage change with state of discharge during discharge and charge.

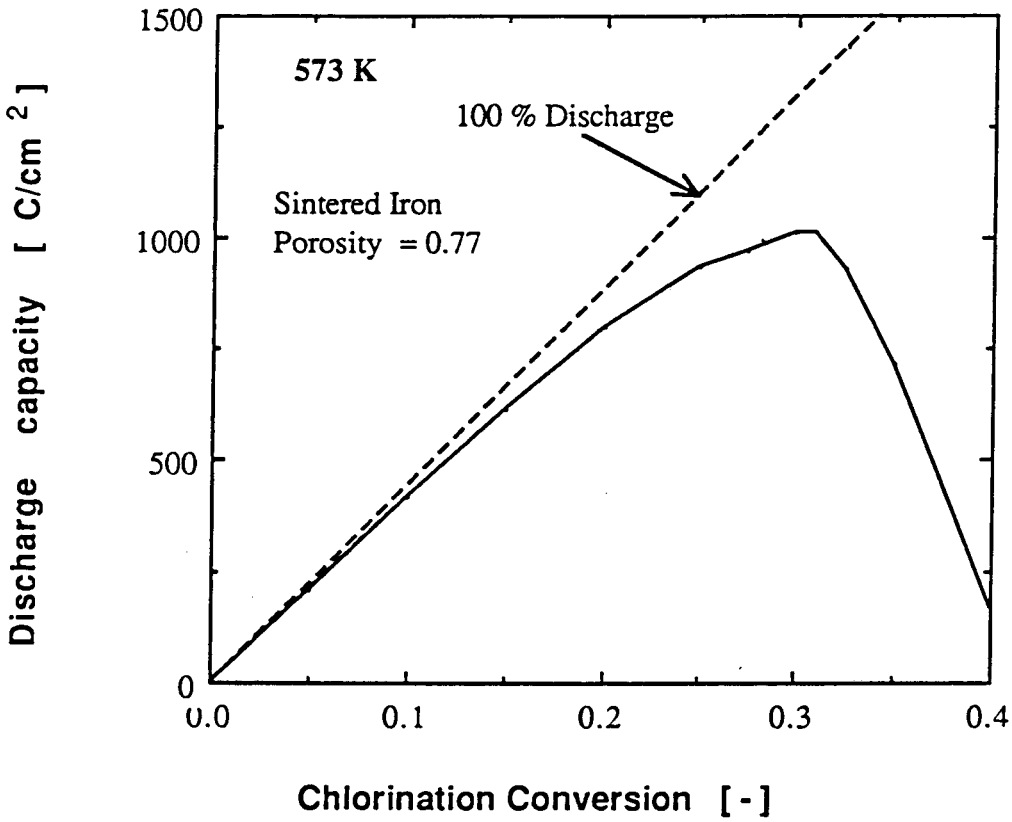

Figure 11. Effect of chlorination conversion of initial sintered iron on discharge capacity.

Conclusion

A mathematical model based on a macroscopic theory of porous electrodes and on transport equations of ionic species with concentrated-solution theory has been presented. This model predicts the concentration profiles of the ionic species in the melt, the porosity distribution, the local reaction rate, and the terminal voltage as functions of the state of discharge. Models assuming no concentration gradient (Model 2), and assuming that the reaction rate is cut off by the disappearance of the NaCl precipitate (Model 3) are compared. The battery performance is mainly affected by the porosity profile, which is dictated by the current density, the precipitation and dissolution rates of NaCl, the concentration of the chloride ion in the melt, the operating temperature, and the initial porosity of the sintered iron. The change in terminal voltage with SOD, when calculated with the model that includes concentration gradients ($k_p = 1.0$), is closer to the voltage change given by Model 3 than the change predicted by Model 2. The voltage drop during discharge is caused by a decrease in the active surface area of the positive electrode; the voltage change during charge is caused by the local disappearance of the NaCl precipitate and by the decrease in the concentration of the chloride ion.

Appendix

Electrode reaction rate including mass transfer—During discharge, the ferrous complex ions are involved with these phenomena:

1. Mass transfer of ferrous complex from the salt surface to the bulk

$$-j = nFk_s a_s (c_{r,e} - c_{r,b}). \tag{A.1}$$

2. Mass transfer of ferrous complex from the bulk to the electrode surface

$$-j = nFk_m a_m (c_{r,b} - c_{r,s}). \tag{A.2}$$

3. Electrodeposition

$$j = i_0 a_m \left\{ \exp\left[\frac{\alpha_a F}{RT}\eta\right] - \frac{c_{r,s}}{c_{r,e}} \exp\left[-\frac{\alpha_c F}{RT}\eta\right] \right\} \tag{A.3}$$

where $i_0 = i_{0,ref} \, (c_{r,e}/c_{r,ref})^{1-\beta} (c_2/c_{2,ref})^{2\beta}$.

Mass transfer coefficient and active surface area.—From an SEM picture of the porous electrode [5], the iron matrix radius, δ_m, is taken to be 1.25 μm, the half of the strip or lamella thickness of iron chloride, δ_s, is 1 μm, and the diffusion coefficient, D, is 5×10^{-6} cm^2/s. The mass transfer coefficients are assumed to be given by

$$k_m = k_m^o \, \epsilon^{1.5} \tag{A.4}$$

and

$$k_s = k_s^o \, \epsilon^{1.5}, \tag{A.5}$$

where k_m^o and k_s^o are derived from D/δ_m and D/δ_s, respectively. The active surface areas of metal and salt in the absence of precipitates are assumed to be

$$a_{m0} = 3\epsilon_{mi}/\delta_m \tag{A.6}$$

and

$$a_{s0} = 3\epsilon_{si}/\delta_s. \tag{A.7}$$

These values are estimated: ϵ_{mi}=0.23, ϵ_{si}=0.4, k_m^o = 0.04 cm/s, k_s^o = 0.05

cm/s, $a_{m0} = 5.52 \times 10^3$ cm^{-1}, and $a_{s0} = 1.20 \times 10^4$ cm^{-1}. The electrode surface area is given by

$$\frac{a_m}{a_{m0}} = \left[\frac{\epsilon_m - \epsilon_{m,max}}{\epsilon_{m0} - \epsilon_{m,max}}\right]^{p_1}\left[1 - \left[\frac{\epsilon_p + \epsilon_s}{1 - \epsilon_m}\right]^{p_2}\right] \qquad (A.8)$$

where $\epsilon_{m,max}$ is the theoretical volume fraction of Fe when the open pore is plugged by maximum charge. The first term on the right side of the equation is the effect of the change in the metal size and the second term is the effect of the covering salt and precipitate. The specific surface area of the salt, $FeCl_2$, is given by

$$\frac{a_s}{a_{s0}} = \left[\frac{\epsilon_s}{\epsilon_{si}}\right]^q. \qquad (A.9)$$

The exponents, p_1, p_2, and q, are assumed to be 2/3.

Electrical conductivity.—The electrolyte components vary with the apparent ratio of NaCl to $AlCl_3$. The reported data [23] of electrolyte conductivity were correlated with the apparent mole fraction m_B of NaCl in the melt:

$$\kappa = 0.1450 - 1.827m_B + (-0.5715 + 6.358m_B)\times 10^{-3}T. \qquad (A.10)$$

The solubility product of NaCl in the melt is described by

$$-\log K_{sp} = -3.770 + 2.690\times 10^3/T - 0.4129\times(10^3/T)^2. \qquad (A.11)$$

The minimum value of m_B, at which the melt becomes saturated with NaCl precipitate, is estimated by

$$m_{B,sat} = 0.8249 - 1.322\times 10^{-3}T + 1.400\times 10^{-6}T^2. \qquad (A.12)$$

The conductivity of the metallic iron is adopted as 3.5×10^4 S/cm.

Molar volume fraction.—The density of the melt was also correlated using the data given in reference [23].

$$\rho = 2.370 - 2.147m_B + 3.197m_B^2 \qquad \text{(A.13)}$$

$$- (2.325 - 7.635m_B + 9.567m_B^2)\times 10^{-3}T.$$

The molar volume of species k is defined by

$$\bar{V}_k = M_k/\rho \qquad \text{(A.14)}$$

where M_k is the molecular weight: $M_A = 191.78$, $M_B = 58.44$. By using Eq. (9), $\bar{V}_e = 112.94$ cm^3/mol, $\bar{V}_A = 121.6$ cm^3/mol, and $\bar{V}_B = 37.06$ cm^3/mol at 300°C.

Diffusion coefficient.—Using the diffusion coefficient of $Al_2Cl_7^-$ in the $NaAlCl_4$ melt at 175°C [24] and the expected temperature dependence [25],

$$D = 4.30\times 10^{-6}\exp\left\{\frac{3.035\times 10^3}{R}\left(\frac{1}{448.15} - \frac{1}{T}\right)\right\}. \qquad \text{(A.15)}$$

Activity coefficient.— The following relationship [26] was used:

$$\ln \gamma_A = \frac{a}{RT}\left(\frac{1-x_A}{1+(b-1)x_A}\right)^2 \qquad \text{(A.16)}$$

where $a/R = 1851$ K and $b = 2.70$.

Acknowledgements

This work was supported by the Assistant Secretary for Conservation and Renewable Energy, Office of Energy Storage and Distribution, Energy Storage Division, U. S. Department of Energy under Contract No. DE-AC03-76SF00098.

List of Symbols

A_L, A_S	areas given by $2\pi r_L H$, $2\pi r_S H$, cm^2
a	interfacial area per unit electrode volume, cm^{-1}
a_i	activity of species i, mol/cm^3
a_m, a_s	specific surface areas of metal and salt, cm^{-1}
C_d	discharge capacity, C/cm^2
c	concentration, mol/cm^3
c_r	concentration of ferrous complex, mol/cm^3
c_T	total concentration, mol/cm^3
D	diffusion coefficient of electrolyte, cm^2/s
F	Faraday's constant, C/mol
f	chlorination conversion
H	height of separator, cm
i_1	superficial current density in matrix phase, A/cm^2
I	current density at separator (negative on discharge), A/cm^2
i_2	superficial current density in electrolyte phase, A/cm^2
i_0	exchange current density, A/cm^2
j	local transfer current, A/cm^3
j_{in}	pore wall flux of species i, $mol/cm^2 \cdot s$
K_{sp}	solubility product of NaCl, mol^2/cm^6
k_m, k_s	mass transfer coefficients of ferrous complex from or to metal, and salt, cm/s
k_p	rate constant of precipitation and dissolution of NaCl, $cm^3/mol \cdot s$
M_i	symbol for chemical formula of species i
M_k	molecular weight of component k, g/mol

m_B	apparent mole fraction of salt B
n	number of electrons transferred in electrode reaction
R	gas constant, J/mol·K
R_I	rate of homogeneous reaction I, mol/cm^3·s
r	radial distance from center of current collector, cm
r_A, r_S	outer and inner diameters of separator, cm
r_L, r_0	outer diameter of positive electrode and diameter of current collector, cm
s_i	stoichiometric coefficient of species i in electrode reaction
T	temperature, K
t	time, s
t_i^r	transference number of species i with respect to reference frame r
U	terminal voltage, V
U_o	open circuit cell voltage, V
ΔU_P	difference of open circuit potential, V
$\bar{V}_e$, $\bar{V}_k$	molar volumes of electrolyte and salt k, cm^3/mol
V_R	electrolyte volume in reservoir, cm^3
v^*	molar average velocity, cm/s
x_k	mole fraction of salt k
z_i	charge number of species i

Greek Letters

α_a, α_c	transfer coefficients
β	symmetry factor
γ	activity coefficient
δ	characteristics length of mass transfer, cm
ϵ	porosity

ϵ_m, ϵ_s, ϵ_p	volume fractions of Fe, $FeCl_2$ and NaCl precipitate
η	total overpotential, V
κ	electrolyte conductivity, S/cm
ρ	density of electrolyte, g/cm^3
σ	metal conductivity, S/cm
ϕ_1	potential in matrix phase, V
ϕ_2	potential in electrolyte phase, V

Subscripts

A, *B*	$NaAlCl_4$, NaCl
b, *e*, *s*	bulk, equilibrium, surface
I	precipitation and dissolution reaction of NaCl
i, 0	initial
max	maximum value
N, *P*, *R*	negative, positive, reservoir
p	NaCl precipitate
ref	reference condition
res, *sep*	reservoir, separator
sat	saturation
1, 2, 3	$AlCl_4^-$, Cl^-, Na^+

Superscripts

c	relative to common ion
P_1, P_2, *q*	exponents
τ	exponent for tortuosity
*	relative to molar average velocity

References

[1] J. Coetzer, "A New High Density Battery System," *J. Power Sources*, 18, 377 (1986).

[2] R. C. Galloway, "A Sodium/Beta-Alumina/Nickel Chloride Secondary Cell," *J. Electrochem. Soc.*, 134, 256 (1987).

[3] R. J. Bones, J. Coetzer, R. C. Galloway, and D. A. Teagle, "A Sodium/Iron(II) Chloride Cell with a Beta Alumina Electrolyte," *J. Electrochem. Soc.*, 134, 2379 (1987).

[4] A. R. Tilley and R. N. Bull, "The Design and Performance of Various Types of Sodium/Metal Chloride Batteries," Proc. 22nd IECEC Meeting, p.1078 (1987).

[5] R. J. Bones, D. A. Teagle, S. D. Brooker, F. L. Cullen, and J. Lumsdon, "An Insight into the Operation of an $Fe/FeCl_2$ Electrode in a Medium Temperature Liquid Sodium/Beta Alumina Cell," *Proceedings of the Second Symposium on Electrode Materials and Processes for Energy Conversion and Storage* (The Electrochemical Society, volume 87-12), p.537 (1987).

[6] J. Newman and W. Tiedemann, "Porous-Electrode Theory with Battery Application," *AIChE J.*, 21, 25 (1975).

[7] J. S. Dunning, *Analysis of Porous Electrode with Sparingly Soluble* Reactants, Dissertation, University of California, Los Angeles, CA (1971).

[8] W. G. Sunu, *Transient and Failure Analyses of a Porous Zinc Electrode*, Dissertation, University of California, Los Angeles, CA (1978).

[9] D. Simonsson, "A Mathematical Model for the Porous Lead Dioxide Electrode," *J. Appl. Electrochem.*, 3, 261 (1973).

[10] K. Micka and I. Rousar, "Theory of Porous Electrode-XI. The Positive Plate of the Lead-Acid Battery," *Electrochim. Acta*, 18, 629 (1973).

[11] W. Tiedemann and J. Newman, "Mathematical Modeling of the Lead-Acid Cell," *Proceedings of the Symposium on Battery Design and Optimization* (The Electrochemical Society, volume 79-1), p.23 (1979).

[12] H. Gu, T. V. Nguyen, and R. E. White, "A Mathematical Model of a Lead-Acid Cell," *J. Electrochem. Soc.*, 134, 2953 (1987).

[13] R. Pollard and J. Newman, "Mathematical Modeling of the Lithium-Aluminum, Iron Sulfide Battery 1. Galvanostatic Discharge Behavior," *J. Electrochem. Soc.*, 128, 491 (1981).

[14] K. Tsaur and R. Pollard, "Mathematical Modeling of the Lithium, Thionyl Chloride Static Cell 1. Neutral Electrolyte," *J. Electrochem. Soc.*, 131, 975 (1984).

[15] K. Tsaur and R. Pollard, "Mathematical Modeling of the Lithium, Thionyl Chloride Static Cell 2. Acid Electrolyte," *J. Electrochem. Soc.*, 131, 984 (1984).

[16] L. G. Boxall, H. L. Jones, and R. A. Osteryoung, "Solvent Equilibria of $AlCl_3$-NaCl Melts," *J. Electrochem. Soc.*, 120, 223 (1973).

[17] R. Pollard and J. Newman, "Transport Equation for a Mixture of Two Binary Molten Salts in a Porous Electrode," *J. Electrochem. Soc.*, 126, 1713 (1979).

[18] J. Newman, *Electrochemical Systems*, Prentice-Hall, Inc., Englewood Cliffs, NJ (1973).

[19] A. C. Buechele, L. C. De Jonghe, and D. Hitchcock, "Degradation of Sodium β"-Alumina: Effect of Microstructure," *J. Electrochemical Soc.*, 130, 1042 (1983).

[20] H. A. Hjuler, A. Mahan, J. H. von Barner, and N. J. Bjerrum, "Chloro Complexes in Molten Salts 9. Potentiometric and Vapor Pressure Study of the System NaCl-$AlCl_3$ in the Temperature Range 175-300°C," *Inorg. Chem.*, 21, 402 (1982).

[21] L. G. Boxall, H. L. Jones, and R. A. Osteryoung, "Electrochemical Studies on Ag, Fe, Cu Species in $AlCl_3$-NaCl Melts," *J. Electrochemical Soc.*, 121, 212 (1974).

[22] A. A. Fannin, Jr., L. A. King, and D. W. Seegmiller, "Chloroaluminate Equilibria in $AlCl_3$-NaCl Melts," *J. Electrochemical Soc.*, 119, 801 (1972).

[23] G. J. Janz, C. B. Allen, N. P. Bansal, R. M. Murphy, and R. P. T. Tomkins, *Physical Properties Data Compilations Relevant to Energy Storage II. Data on Single and Multi-Component Salt Systems*, p. 266 NBS

(1979).

[24] P. Rolland and G. Mamantov, "Electrochemical Reduction of $Al_2Cl_7^-$ Ions," *J. Electrochemical Soc.*, 123, 1299 (1976).

[25] N. G. Chovnyk and M. V. Myshalov, "Polarogram of Reduction of Ferric to Ferrous Ions in the Fused System $AlCl_3$-NaCl," *Soviet Electrochem.*, 6, 1583 (1970).

[26] H. Linga, K. Motzfeldt, and H. A. Oye, "Vapour Pressure of Molten Alkali Chloride-Aluminum Chloride Mixtures," *Ber. Bunsenges. Phys. Chem.*, 82, 568 (1978).

LAWRENCE BERKELEY LABORATORY
TECHNICAL INFORMATION DEPARTMENT
1 CYCLOTRON ROAD
BERKELEY, CALIFORNIA 94720